

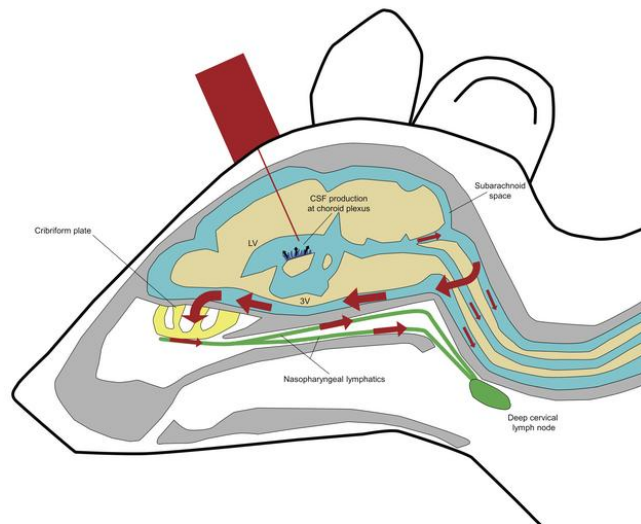
## Magnetic resonance imaging of cerebrospinal fluid outflow after low-rate lateral ventricle infusion in mice

Yann Decker, ... , Klaus Fassbender, Steven T. Proulx

*JCI Insight*. 2021. <https://doi.org/10.1172/jci.insight.150881>.

Resource and Technical Advance In-Press Preview Neuroscience Vascular biology

### Graphical abstract



Find the latest version:

<https://jci.me/150881/pdf>



1  
2  
3  
4  
5  
6  
7 Magnetic resonance imaging of cerebrospinal fluid outflow after  
8 low-rate lateral ventricle infusion in mice  
9

10  
11  
12  
13 Yann Decker<sup>1</sup>, Jonas Krämer<sup>1</sup>, Li Xin<sup>2</sup>, Andreas Müller<sup>3</sup>, Anja Scheller<sup>4</sup>, Klaus  
14 Fassbender<sup>1</sup>, Steven T. Proulx<sup>2</sup>  
15

16  
17  
18  
19 <sup>1</sup>Department of Neurology, Saarland University Medical Center, Homburg, Germany

20 <sup>2</sup>Theodor Kocher Institute, University of Bern, Bern, Switzerland

21 <sup>3</sup> Clinic for Diagnostic and Interventional Radiology, University of the Saarland,  
22 Homburg, Germany

23 <sup>4</sup> Molecular Physiology, Center for Integrative Physiology and Molecular Medicine  
24 (CIPMM), University of Saarland, Homburg, Germany  
25

26  
27 The authors have declared that no conflict of interest exists.  
28

29  
30 Corresponding authors:  
31

32 Yann Decker, PhD  
33 Department of Neurology  
34 Saarland University Medical Center  
35 66421 Homburg/Saar, Germany  
36 Tel.: ++49-6841-1624215  
37 Email: [yann.decker@uks.eu](mailto:yann.decker@uks.eu)  
38

39 Steven T. Proulx, PhD  
40 Theodor Kocher Institute  
41 University of Bern  
42 CH-3012 Bern, Switzerland  
43 Tel.: ++41-31-631-5390  
44 Email: [steven.proulx@tki.unibe.ch](mailto:steven.proulx@tki.unibe.ch)

45 Abstract

46

47 The anatomical routes for the clearance of cerebrospinal fluid (CSF) remain incompletely  
48 understood. However, recent evidence has given strong support for routes leading to  
49 lymphatic vessels. A current debate centers upon the routes through which CSF can  
50 access lymphatics, with evidence emerging for either direct routes to meningeal  
51 lymphatics or along cranial nerves to reach lymphatics outside the skull. Here, a method  
52 was established to infuse contrast agent into the ventricles using indwelling cannulae  
53 during imaging of mice at 2 and 12 months of age by magnetic resonance imaging. As  
54 expected, a significant decline in overall CSF turnover was found with aging.  
55 Quantifications demonstrated that the bulk of the contrast agent flowed from the ventricles  
56 to the subarachnoid space in the basal cisterns. Comparatively little contrast agent signal  
57 was found at the dorsal aspect of the skull. The imaging dynamics from the two cohorts  
58 revealed that the contrast agent cleared from the cranium through the cribriform plate to  
59 the nasopharyngeal lymphatics. On decalcified sections, we confirmed that fluorescently-  
60 labeled ovalbumin drains through the cribriform plate and can be found within lymphatics  
61 surrounding the nasopharynx. In conclusion, routes leading to nasopharyngeal  
62 lymphatics appear to be a major efflux pathway for cranial CSF.

63

64

65

66

67

68 Keywords:

69

70

71 Cerebrospinal fluid, lymphatic vessel, contrast enhanced-magnetic resonance imaging,  
72 clearance, aging

73

74

75

76

77

78

79

80

81

82

83

84

85

86

87

88

89 **Introduction**

90

91 Cerebrospinal fluid (CSF) is produced within the ventricles by the choroid plexuses and  
92 circulates within the subarachnoid spaces around the brain and spinal cord. Historically,  
93 it was concluded that CSF would leave the central nervous system (CNS) via direct  
94 pathways through outcroppings of arachnoid tissue into the venous sinuses of the dura  
95 mater (1, 2). However, in recent decades it has become commonly accepted that  
96 lymphatic vessels play a significant role in the process of CSF drainage (3-6). Recent  
97 studies in rodents have demonstrated that lymphatic vessels appear to be the exclusive  
98 clearance route for tracers injected into the CSF, even for small molecular weight solutes  
99 (7, 8). An active area of research has focused upon the anatomical routes of outflow that  
100 CSF takes to access the lymphatic vessels. Support exists for access of CSF to lymphatic  
101 vessels that have been recently rediscovered in the dura mater (9-11) and for efflux along  
102 cranial or spinal nerves to reach extracranial lymphatics (7, 12-15). Of the perineural  
103 routes, evidence in many different species exists for routes along olfactory nerves through  
104 the cribriform plate (5, 10, 16-20).

105

106 Imaging techniques have long been utilized to assess CSF outflow of tracers (6).  
107 Traditionally, these techniques have employed X-ray or scintigraphic measurements (21,  
108 22). Recently, two-photon or near-infrared fluorescence techniques (7-9, 13, 14, 23) have  
109 been developed to allow sensitive in vivo readouts within the CNS (imaging through-skull  
110 or through-spine), to specific efflux pathways (imaging through vomeronasal bones into  
111 the nasal region or imaging of lymphatic vessels draining to the superficial cervical or  
112 mandibular lymph nodes) or as a readout for transport to blood from multiple pathways.  
113 However, these methods can only allow assessments at one particular region at a  
114 relatively superficial level. On the other hand, contrast enhanced-magnetic resonance  
115 imaging (CE-MRI) techniques have the advantage of 3D imaging of the entire cranial or  
116 spinal regions in the context of the surrounding soft-tissue anatomy, with sufficient  
117 temporal resolution to track the dynamics of contrast agent outflow, and have a more  
118 immediate translational potential to the clinic (8, 11-13, 15, 24).

119

120 One valid criticism of tracer injection studies is that they may inherently introduce artifacts  
121 due to relatively large acute volumes introduced into the CSF. In the mouse, with an  
122 estimated CSF volume of 35  $\mu$ L (2), injections of 5 to 10  $\mu$ L made within a short period  
123 likely introduce elevated pressure conditions that will affect the dynamics and routes of  
124 outflow (8, 25). Our group has attempted to address this issue by establishment of an  
125 indwelling cannula into the lateral ventricle of mice that allows slow infusion during  
126 imaging acquisition (13) at rates below the published rates for CSF production (2, 26).  
127 We have utilized this cannula system to allow MRI measurements of spinal CSF  
128 distribution and sacral outflow during the infusion of contrast agent (13). Similar cisterna  
129 magna infusion setups have also recently been employed by other groups to examine  
130 cranial CSF distribution (12, 15).

131

132 Alterations in CSF circulation may have significant effects on the pathogenesis of  
133 neurological conditions associated with the aging process, including dementia and stroke.  
134 Many research groups have now demonstrated that a slower overall efflux of CSF occurs  
135 during the aging process (7, 11, 14). Thus, we have utilized this expected difference in  
136 CSF turnover dynamics between younger (2-3 month old) and older (12 month old) mice  
137 to aid in validation of MRI quantifications. Second, we have investigated potential efflux  
138 routes by analyzing the contrast agent signal dynamics at several different locations  
139 within the CNS and the draining cranial lymph nodes. We hypothesized that differences  
140 in signal dynamics quantified between the two age groups will be apparent only at the  
141 major site(s) of efflux.

142

143

## 144 **Results**

145

### 146 **Tracer infused into the lateral ventricle follows a continuous outflow route from the** 147 **nasal cavity to the draining cervical lymph nodes**

148

149 Since CSF is principally produced by the choroid plexuses that are located in the  
150 ventricles, we decided to analyze the flow of tracer following an intraventricular low-rate  
151 infusion of a 17 kDa dendritic gadolinium-based contrast agent, Gadospin D (Fig. 1a). We  
152 chose Gadospin D rather than a low molecular weight contrast agent to limit potential  
153 diffusion into the brain parenchyma from the ventricular injection site. After stereotactic  
154 implantation of an indwelling cannula in the right lateral ventricle, mice were positioned in  
155 a prone position on a horizontal MRI platform. A polyethylene line filled with contrast agent  
156 was subsequently connected at one end to the cannula and at the other end to an infusion  
157 pump. After a baseline pre-contrast scan, an infusion of the contrast agent was started at  
158 a rate of 0.1  $\mu$ l/min for 60 min and a series of CE-MRI images were collected over the  
159 course of 90 min. This experimental setup allowed us acquire images of the animal  
160 throughout the course of the infusion of a macromolecular contrast agent at rates not  
161 excessive to physiological levels.

162

163 We first determined the general pattern of the spread of Gadospin D by generating  
164 maximum intensity projection images at each timepoint to allow a 3D dynamic  
165 visualization of the contrast agent (Video 1). An initial filling of the ventricular system was  
166 apparent with spreading ventrally to the basal cisterns and under the olfactory bulbs within  
167 the first 15 min after the start of the infusion. With increasing time, it was observable that  
168 the signal intensity of the tracers was progressively detectable in the nasal cavity, in the  
169 nasopharyngeal region and in the deep and superficial lymph nodes (Fig. 1b). Moreover,  
170 as observable in Fig. 1c and Video 1, it was possible to identify a continuous anatomic  
171 route along the nasopharynx that emerged from the nasal cavity and connected to the  
172 deep cervical lymph nodes. Connections also were apparent from the deep cervical  
173 lymphatics to the superficial cervical (or mandibular) lymph nodes, as previously shown  
174 using near-infrared imaging (7).

175

176 **Reduced tracer clearance from the ventricles and slower efflux to draining lymph**  
177 **nodes in older mice**

178  
179 It has recently been demonstrated that CSF production and drainage are both reduced in  
180 aged mice suggesting that the overall CSF turnover is slower with aging (7, 14, 27).  
181 During and immediately after the low-rate intraventricular infusion, we investigated the  
182 clearance of Gadospin D from the ventricular system in two groups of mice of either 2-3  
183 months (n=7) or 12 months of age (n=6). While the low rate infusion of contrast agent  
184 took place during the first 60 min, we observed that the signal intensity in the contralateral  
185 ventricles reached a peak at around 40 min and then progressively decreased in both  
186 age groups (Fig. 2a; Supp Fig.1a). At later timepoints, we could observe significantly  
187 stronger decreased signal intensity in the contralateral ventricle of the group of younger  
188 mice. As no significant difference was observed in the volume of the contralateral  
189 ventricles (Fig. 2b) between the two groups, we concluded that a decrease in the rate of  
190 CSF turnover is responsible for the reduced contrast agent clearance observed in the 12  
191 month old mice.

192  
193 Our previous studies have shown that lymphatic outflow from CSF is reduced in 18 month  
194 old mice compared to 2 month old mice following a bolus injection of a macromolecular  
195 fluorescently-labeled tracer (7). We tested whether this difference would be apparent by  
196 MRI in mice of 12 months of age by quantifying the signal intensity of the contrast agent  
197 in regions-of-interest (ROIs) positioned in the deep and superficial cervical lymph nodes.  
198 Dynamic CE-MRI quantification revealed less contrast agent signal in both groups of  
199 cervical lymph nodes in the 12 month old mice compared to the group of younger mice  
200 (Fig. 2c,d; Supp Fig.1b,c). Quantifications of the volume of 3D reconstructions of the  
201 cervical lymph nodes also did not show significant differences between the two age  
202 groups (Supp Fig.1d,e).

203  
204 In sum, we observed that with aging, a low-rate infusion of a macromolecular contrast  
205 agent is associated with reduced clearance from the ventricles and a delayed transport  
206 to draining lymph nodes which is consistent with previous studies by our group and others.  
207 Thus, we next aimed to exploit these differences in CSF turnover dynamics between the  
208 two age groups of mice to help identify the major efflux routes from the ventricular system  
209 to the lymphatic system.

210  
211 **Contrast agent flows along the ventral aspect of the brain and down the spine**

212  
213 CSF has recently been proposed to reach the dura mater on the dorsal aspect of the skull  
214 where it is hypothesized to be either directly or indirectly drained by meningeal lymphatic  
215 vessels leading to the deep cervical lymph nodes (9, 28-30). Previous work has  
216 highlighted lymphatic vessels in the dural tissue surrounding the sagittal and the  
217 transverse sinuses to be “hotspots” for uptake from the CSF. Thus, following  
218 intraventricular infusion of Gadospin D, we quantified the signal intensity in two ROIs of  
219 the dorsal aspect of the skull in proximity to these regions. In both areas, we could

220 observe only a limited maximum change in signal intensity compared to baseline (sagittal  
221 sinus ROI: <42%; quadrigeminal cistern ROI: < 120%) and no significant differences at  
222 any timepoint between the groups of 2 month and 12 month old mice (Fig 3 a,b,c; Supp  
223 Fig.2 a,b).

224  
225 On the other hand, quantifications of ROIs in the ventral region (at the basal cisterns  
226 around the circle of Willis and the internal carotid artery) show a substantial increase in  
227 maximum change in signal intensity compared to baseline (CoW ROI: >700%; Internal  
228 carotid ROI: >700% ) suggesting that this area is the major site of contrast agent bulk flow  
229 (Fig 3 a,d,e; Supp Fig.2 c,d). Moreover, in the two regions investigated the signal intensity  
230 was significantly quantitatively higher at earlier time points in young mice compared to  
231 the group of 12 month old mice. These results indicate that an infused macromolecular  
232 tracer principally flows with the CSF through the ventral, rather than dorsal, aspect of the  
233 skull.

234  
235 As CSF leaving the ventricles has free communication with the subarachnoid space  
236 around the spinal cord, we also quantified the dynamics in the ventral aspect of the  
237 cervical spine (Supp Fig.3a). We observed a rapid increase in signal intensity in the group  
238 of young mice that reached a maximum percentage change of more than 600%.  
239 Conversely, in the group of 12 month old mice, the signal intensity increase was delayed  
240 and only reached approximately half of the value observed in young mice. Thus, CSF  
241 tracer flow from the ventricular system to the spine can be easily demonstrated with CE-  
242 MRI and exhibits the expected decline with aging.

243  
244 Recent work has introduced the concept of glymphatic flow that would theoretically aid in  
245 CSF/solute penetration into the brain parenchyma along paraarterial spaces. Recent MRI  
246 studies have shown that low molecular weight contrast agents, such as gadoteric acid  
247 (Gd-DOTA), do indeed demonstrate signal enhancement within the parenchyma (31-36).  
248 However, we were unable to confirm a significant influx of the Gadospin D contrast agent  
249 (17 kDa) into the brain cortex in either group (maximum percentage change of 17%). This  
250 limited signal enhancement of a macromolecular contrast agent within the brain is  
251 consistent with our earlier study (8) and others (12).

252  
253 Thus, we conclude from this study that bulk flow routes to the basal cisterns and the  
254 subarachnoid space of the spinal canal are the major pathways for CSF macromolecular  
255 distribution from the ventricular system.

### 256 257 **Dynamics of CSF contrast agent outflow support route(s) leading to the** 258 **nasopharyngeal lymphatics**

259  
260 After observing that a significant portion of the tracer reaches the basal cisterns, we aimed  
261 to elucidate the potential anatomical pathways from this location that might be used to  
262 reach the cervical draining lymph nodes. Based on our observation that the bulk of the  
263 contrast agent appeared to flow continuously from the region of the olfactory bulbs to the

264 nasopharynx and to the draining lymph nodes, we first quantified the changes in signal  
265 intensity in ROIs localized in the nasal turbinates and the nasopharynx (Fig 4 a,b,c; Supp  
266 Fig.4 a,b). Dynamic imaging showed in the group of 12 month old mice, a delayed and  
267 significantly reduced transport of contrast agent in these two regions.

268

269 At other regions suggested to be efflux sites from the skull, CSF contrast agent signal  
270 could be detected in the jugular region below the skull and around the optic nerves (Fig  
271 4 a,d,e; Supp Fig.4 c,d). However, at these two regions, our quantifications revealed that  
272 no significant differences in the signal intensity at any time point were observed between  
273 the young and 12 month old groups. In fact, the jugular region appeared to show a trend  
274 towards increased signal intensity over time in the 12 month old mice compared to the  
275 young mice indicating that this region may be a site of accumulation of contrast agent. An  
276 earlier report has shown that dural lymphatic vessels of this region become more  
277 hyperplastic with age (11).

278

279 Thus, as the expected differences in signal dynamics between young and older animals  
280 were only detectable in the nasal turbinate and the nasopharyngeal areas, we conclude  
281 that this route is one of the major pathways for CSF clearance from the cranium to the  
282 cervical lymph nodes.

283

### 284 **Histological confirmation of CSF outflow route(s) to the nasopharyngeal** 285 **lymphatics**

286

287 Interestingly, the signal quantifications revealed that only a minimal increase of signal  
288 (170% in young mice, 85% in 12 month old mice) could be detected within the turbinates  
289 themselves in either group, whereas much larger signal increases were detected at the  
290 nasopharynx (710% in young mice, 570% in 12 month old mice). This may suggest that  
291 the contrast agent distributes to a large area throughout the nasal cavity after effluxing  
292 through the cribriform plate before draining to the lymphatic vessels near the nasopharynx  
293 leading to the lymph nodes, as appears to be evident from the sagittal view in Video 1.

294

295 To further evaluate how CSF tracers drain through the cribriform plate to reach lymphatics  
296 surrounding the nasopharynx, we have injected AlexaFluor647-labeled ovalbumin  
297 (AF647-OVA) using the same slow infusion protocol employed within the MRI and have  
298 assessed the presence of tracer on sections from decalcified craniums and deep cervical  
299 lymph nodes. Lymphatic vessels have been identified using LYVE-1 antibodies. As seen  
300 in Figure 5a,b taken from two coronal sections at different levels of the nasal cavity,  
301 AF647-OVA is clearly associated with olfactory nerves crossing the cribriform plate and  
302 is distributed throughout a wide volume of nasal mucosal tissue. A rich network of LYVE1+  
303 lymphatic vessels exists laterally on both sides of the nasopharynx and these vessels  
304 could be found containing AF647-OVA signal (Figure 5c-e). Deep cervical lymph nodes  
305 located downstream of this site also contained AF647-OVA that was found within LYVE-  
306 1+ lymphatic sinuses (Figure 5f-j). Thus, this serves as histological confirmation of the  
307 CSF drainage route visible on the MRI.



308 **Discussion**

309

310 In this study, we have assessed CSF outflow by MRI in two different age groups (2-3  
311 months and 12 months) of mice by utilizing an indwelling catheter system to allow low-  
312 rate infusion of a macromolecular contrast agent during a series of image acquisitions.  
313 Similar to previous reports, we found slower dynamics of CSF circulation in the older  
314 cohort of mice compared to the younger mice. Imaging of the contrast agent dynamics in  
315 the cranial region revealed that the bulk of the CSF flowed ventrally under the brain  
316 through the basal cisterns and exited through the cribriform plate to be collected by  
317 lymphatics in the nasopharyngeal region.

318

319 Our methods are similar to those within recent publications utilizing MRI for examination  
320 of CSF flow in rodents (11, 12, 15). In these studies, the authors infused contrast agents  
321 within the MRI into the cisterna magna through a cannula and examined the efflux routes  
322 from the cranial cavity. In our study, we chose to infuse into the ventricles, close to the  
323 source of production at the choroid plexuses, which allowed assessment of the clearance  
324 from the ventricular system, as well as distribution to and efflux from the subarachnoid  
325 space.

326

327 We observed minimal contrast agent signal in the dorsal region near the dural sinuses or  
328 above the cortical hemispheres. Thus, this is contrary to a concept of a major pathway of  
329 CSF outflow at the dorsal dura, as proposed in several recent studies in mice (9, 28, 29)  
330 and recently extended to the human situation (37). Instead, the dynamics clearly indicated  
331 that the majority of contrast agent traversed the basal cisterns with pathways from the  
332 cisterna magna to the subarachnoid space around the circle of Willis. This is consistent  
333 with both historical data (1, 38) and other recent MRI studies (8, 11, 12, 15, 24, 33). While  
334 it is clear that some portion of CSF does reach the surface of the cortical hemispheres as  
335 well as the subarachnoid cisterns located near the dural sinuses (12, 13, 39, 40) the  
336 significance and ultimate egress route(s) for this flow remain open questions.

337

338 As we anticipated, our data indicates that there is a reduction in CSF outflow in older mice  
339 consistent with previous reports (7, 11, 14, 41). We were able to detect delays in 12  
340 month-old animals in CSF clearance and transport at several locations along the CSF  
341 flow pathways, including the lateral ventricle, basal cisterns, cervical spinal subarachnoid  
342 space, nasal turbinates, nasopharyngeal lymphatics and CNS-draining lymph nodes.  
343 Thus, the data is indicative of an overall reduction in CSF turnover with aging. The reason  
344 for this diminished turnover of CSF is not yet clear, however, it may be related to a  
345 reduced CSF production by the choroid plexuses (27, 42), morphological changes in the  
346 dural lymphatics (11) or a reduced transport within lymphatic vessels outside the CNS  
347 (43-45). Whether this slowed CSF circulation plays a role in the development of  
348 neurodegenerative disorders associated with aging, as speculated in many recent studies  
349 (11, 46), remained to be determined.

350

351 We took advantage of the differences in contrast agent dynamics between the two  
352 different age groups of mice to attempt to elucidate the relative importance of several  
353 potential efflux routes. We hypothesized that only along the major bulk flow pathways for  
354 CSF egress would the patterns of contrast agent dynamics between the two age groups  
355 mirror those seen at the downstream lymph nodes. Since we found that limited contrast  
356 agent signal was apparent along the dorsal aspect of the skull, we focused these efforts  
357 on potential efflux routes from the basal cisterns. From this location, evidence exists in  
358 the literature for outflow to the lymphatic system through the cribriform plate (1, 5, 7, 16,  
359 17, 19, 47), along the sheaths surrounding the optic nerves (7, 48, 49), through the jugular  
360 foramina (7, 10, 11, 15, 47) and from the spinal column (13, 23, 50). Of these routes, in  
361 our study only the spinal and nasal regions appeared to exhibit the expected contrast  
362 enhancement dynamics between the two age groups of mice. An outflow pathway to the  
363 lymphatic system does indeed exist in rodents from the sacral region of the spine,  
364 however, our previous work and others have determined that under normal conditions the  
365 spinal pathways are minor compared to the cranial efflux routes (13, 51, 52). Thus, the  
366 resulting conclusion of a major CSF outflow pathway through the cribriform plate would  
367 be in agreement with many previous studies (14, 18, 53, 54). Strong supporting evidence  
368 for this conclusion comes from experiments blocking this pathway which resulted in  
369 dramatic decreases in tracer recovery outside the CNS and increased intracranial  
370 pressure during fluid challenge (53, 55). However, we cannot rule out at this point that  
371 more direct pathways may exist from the basal skull to reach the nasopharyngeal  
372 lymphatics.

373  
374 This conclusion appears to conflict with that of Ahn et al. in rats who determined using  
375 MRI imaging with a macromolecular contrast agent that basal meningeal lymphatic  
376 vessels draining through the jugular foramina are the major route for CSF macromolecular  
377 uptake and drainage. It must be noted that in their study Ahn et al. did not investigate any  
378 potential efflux through the cribriform plate region. However, another possible explanation  
379 for this discrepancy may be due to different experimental conditions between our study  
380 and Ahn et al. In a recent elegant MRI study by Stanton et al, the authors have  
381 demonstrated that the choice of anesthesia has a significant effect on the amount of efflux  
382 through the cribriform plate, with mice under isoflurane anesthesia demonstrating much  
383 less Gd-DTPA signal in this area (15). This study is consistent with earlier work  
384 demonstrating differences in CSF flow dynamics under different types of anaesthesia (8,  
385 13, 56). The authors demonstrated that mice under 1.5% anesthesia exhibited more  
386 signal at the jugular foramina along the cranial nerves and also to the spinal canal,  
387 indicating that shunting of the CSF flow may occur under certain conditions (15). This  
388 potential redirection of flow is an important factor to consider, especially in the context of  
389 pathological conditions such as hydrocephalus or glioblastoma, which may block CSF  
390 outflow pathways at the skull and reroute flow to the spine (57, 58).

391  
392 The situation in humans remains unresolved (6). Studies have presented evidence both  
393 for and against efflux of contrast agent through the cribriform plate (54, 59-61). One recent  
394 clinical MRI study has concluded that CSF efflux to the nasal region is minimal in humans

395 (61). This paper used a low molecular weight gadolinium contrast agent injected into the  
396 lumbar intrathecal space and examined the nasal turbinates at multiple timepoints in  
397 patients with various CSF disorders. Although contrast agent was observable in almost  
398 half the patients below the cribriform plate along the olfactory nerves, the authors were  
399 unable to observe a significant increase of signal within the nasal cavity at any time point.  
400 Our current study demonstrates the technical difficulty of detecting significant contrast  
401 agent signal enhancement within nasal tissue using an MRI approach, even though we  
402 employed a macromolecular contrast agent that should be expected to clear exclusively  
403 from the nasal submucosa through lymphatics (53). While the exact anatomical routes  
404 remain to be elucidated, it is evident from our decalcified sections after ovalbumin infusion  
405 that the contrast agent spreads throughout a wide volume of the nasal tissue after  
406 crossing the cribriform plate, which may partially account for the difficulty in detecting  
407 signal with MRI in humans.  
408

409 In sum, through establishment of a technique allowing dynamic CE-MRI under low-rate  
410 infusion of gadolinium contrast agents, we conclude that CSF distributes from the  
411 ventricles to the subarachnoid space ventral to the brain and in a caudal direction down  
412 the spine. Under our experimental conditions, a significant outflow route from the cranium  
413 appeared to be through the nasal region to reach lymphatic vessels near the nasopharynx  
414 before draining to the cervical lymph nodes. With aging, the dynamics of clearance from  
415 the ventricles and flow through the nasal tubinates and nasopharyngeal lymphatics to the  
416 lymph nodes were reduced. These experiments have set the stage for further MRI  
417 evaluation of CSF outflow in mouse models of neurological disorders.  
418  
419

## 420 **Methods**

### 421 **Mice**

422 Female wild-type mice (Janvier, France) on the C57BL/6 background were kept under  
423 specific pathogen-free conditions until they were used for experimental studies.

### 424 **Surgical preparation**

425 Mice were anesthetized by intraperitoneal injection of 100 mg/kg ketamine and 20 mg/kg  
426 xylazine and fixed in a stereotaxic frame (Kopf Instruments, Tujunga, CA). Under this  
427 narcosis, the skull was thinned with a Proxxon GG 12 Engraving drill (Proxxon, Niersbach,  
428 Germany). A 28G, 2.5-mm-long MRI-compatible microcannula (#328OP/PK/Spc; Plastics  
429 One) was inserted stereotactically 0.95 mm lateral and 0.22 mm caudal to the bregma  
430 and 2.50 mm ventral to the skull surface (13). The microcannula was sealed with  
431 cyanoacrylate glue. Animals were transferred into the magnet in a prone position on an  
432 MRI cradle (BioSpec Avance III 94/20; Bruker Biospin GmbH, Ettlingen, Germany). A 1-  
433 1.5m long polyethylene catheter filled with a Gadospin D (nanoPET Pharma GmbH,  
434 Germany) solution at a Gd concentration of 25 mM was connected to the MRI compatible

435 microcannula and a 10- $\mu$ l syringe operated by an MRI compatible NanoJet syringe pump  
436 (Chemyx Inc., Stafford, TX, USA). The skin incision was then closed with a medical  
437 adhesive bandage around the cannula and the catheter. Animals were allowed to breathe  
438 spontaneously during the entire experimental procedure. Respiratory rate and  
439 temperature were measured with non-invasive probes (SA Instruments, Stony Brook,  
440 NY). Throughout the experiment, the body temperature was maintained between 36.5°C  
441 and 37.5°C. During the course of the MRI measurement, the initial narcotic was  
442 supplemented as necessary with 0.5-1% isoflurane delivered in 98% O<sub>2</sub> to keep the  
443 breathing rate lower than 140 breaths per min.

#### 444 Dynamic contrast-enhanced MRI of the head-neck

445 Animals were examined in a horizontal-bore 9.4 T animal scanner (BioSpec Avance III  
446 94/20; Bruker Biospin GmbH, Ettlingen, Germany) with a BGA12S gradient system with  
447 ParaVision 6.0.1 (Bruker Biospin GmbH) and a linearly polarized coil with an inner  
448 diameter of 40 mm (Bruker Biospin GmbH). Contrast-enhanced imaging was achieved  
449 with a three-dimensional time of flight gradient recalled echo sequence (3D-TOF-GRE)  
450 originally adapted for imaging of peripheral lymph vessels (62) with a recovery time of  
451 12.0 ms, echo time = 2.5 ms, flip angle = 25°, a matrix of 600 × 432 × 180, field of view  
452 36.00 mm × 25.92 mm × 18.00 mm, 1 average and a scan time of 4 min 19 s 200 ms. A  
453 phantom placed in the vicinity of the animal's head (solution diluted in 0.9% NaCl at 5 mM  
454 gadolinium) was used for image intensity normalization over the time series. Following a  
455 pre-contrast scan, a Gadospin D solution at 25 mM Gd was infused at a constant rate of  
456 0.1  $\mu$ l/min for 60 min. Total scan time was between 95 and 99 min.

457

#### 458 Data processing

459 ROIs were manually drawn around the different anatomical regions investigated with  
460 Horos (version 3.3.6, Horos Project). Signal intensity was normalized using the reference  
461 phantom. The normalized ROI value (provided in the supplemental data) was calculated  
462 by dividing the original ROI value by the phantom value of the same scan. Contrast agent  
463 efflux over time was determined by calculating the percentage change of signal intensity  
464 as a function of time after infusion of the contrast agent using the following equation:  
465  $[(\text{normalized signal intensity} - \text{normalized pre-contrast intensity}) / (\text{normalized pre-}$   
466  $\text{contrast intensity})] \times 100$ . Ventricle and lymph node volumes were quantified using semi-  
467 automatic segmentation tools in 3DSlicer, version 4.11 ([www.slicer.org](http://www.slicer.org)). All the digital  
468 imaging and communications in medicine images were imported into 3D Slicer for the  
469 segmentation and 3D modelling. The region of interest was first defined and segmented  
470 with the segment editor module. The model maker module was used to create the 3D  
471 model. Finally, the volume was determined via the segment statistics module.

472

#### 473 Histological analysis of tracer efflux to lymphatics

474 For experiments where ventricular infusions were followed by histological analysis an  
475 identical procedure was used with the following modifications: a solution of ovalbumin-  
476 Alexa647 (Thermo Fisher Scientific, Waltham, MA, USA) dissolved in artificial CSF  
477 (Harvard Apparatus, Holliston, MA, USA) at a concentration of 5 mg/mL was infused at a  
478 constant rate of 0.1  $\mu$ L/min for 60 min; the 2-3 months wild-type mice were sacrificed at  
479 the end of the infusion.

480 For decalcification, intracardiac perfusion with PBS and 4% PFA was performed.  
481 Afterwards, the mice were decapitated followed by the removal of skin, muscles, incisors  
482 and lower jaw from the cranium. The cranium was then immersed in 4% PFA for overnight  
483 fixation before being placed in 14% EDTA for 7 days (refreshed daily) at 4°C. Decalcified  
484 tissue was then immersed in 30% sucrose for 3 days for cryoprotection before OCT  
485 embedding. 20 $\mu$ m-thick coronal sections were cut from a cryostat (Cryostar NX50) and  
486 stored at -80°C. For immunofluorescence staining of LYVE-1, frozen tissues were first  
487 hydrated with PBS for 10 minutes, then permeabilized by 0.1% triton for 10 minutes. 10%  
488 goat serum was used for blocking for 1 hour at room temperature. Tissues were incubated  
489 with primary antibody (rabbit anti-Lyve-1, AngioBio, catalogue 11-034, 1:600 dilution) for  
490 3 hours at room temperature and then washed with PBS before incubating with secondary  
491 antibody (goat anti-rabbit Alexa488) for 2 hours at room temperature. Imaging of the nasal  
492 region was done under Zeiss Axiozoom V16 microscope equipped with a Photometrics  
493 PrimeBSI sCMOS camera combined with a LED illumination system pe-4000 and ZEN 2  
494 software (Carl Zeiss). Higher magnification images were then acquired using a Zeiss  
495 LSM800 confocal microscope.

496 For processing of draining lymph nodes, cervical lymph nodes were post-fixed in 4% PFA  
497 at 4°C overnight. Lymph nodes were further immersed in 30% sucrose for 2 days at 4°C  
498 before being snap-frozen in melting isopentane with liquid nitrogen. The frozen tissue was  
499 cut serially into 15  $\mu$ m sections with a cryostat microtome (Leica Microsystems, Wetzlar,  
500 Germany). Sections were incubated with an anti-LYVE-1 (eBioscience, San Diego, CA,  
501 USA, clone ALY7, 1:200) primary antibody for 2 hours at room temperature before  
502 incubation with a Donkey anti-rat (Invitrogen, Grand Island, NY, 1:1000) secondary  
503 antibody conjugated with Alexa488 for 1 hour at room temperature. Sections were finally  
504 counterstained with DAPI. Regions of interest were acquired with a Zeiss LSM 880 Axio  
505 Observer.

## 506 Statistics

507 Statistical analyses were performed with GraphPad Prism 5 (GraphPad). Graphs  
508 represent mean  $\pm$  SEM. Means of two groups were compared using an unpaired two-  
509 tailed Student's t test. Two-way ANOVAs were used for comparison with time points being  
510 a within-subject factor and age being a between-subject factor, followed by Bonferroni's  
511 posthoc test. A p-value <0.05 was considered statistically significant.

512

## 513 Study approval

514 All mouse experiments were approved by the Landesamt für Gesundheit und  
515 Verbraucherschutz, Saarbruecken, Germany (license numbers 31/2018 and 45/2019).

516

517

### 518 **Author contributions**

519 Y.D. and S.T.P. conceived and designed the study. Y.D. performed the MRI experiments.  
520 Y.D., L.X. and A.S. performed the histology experiments. J.K., Y.D and S.T.P. analyzed  
521 the data. A.M. and Y.D. applied for approval of animal experiments. A.M. maintained the  
522 MRI facility. K.F. made substantial contributions to the conception of the study. Y.D. and  
523 S.T.P drafted the manuscript. All authors have approved the final version of the  
524 manuscript and have agreed to be accountable for all aspects of the work.

### 525 **Acknowledgements**

526 We also thank Prof. Walter J. Schulz-Schaeffer for his critical reading of the manuscript.  
527 The authors also thank Prof. Arno Bücker and Prof. Michael D. Menger for their support  
528 of the MRI facility. This work was supported by the Medical Faculty of the University of  
529 the Saarland (HOMFOR 2019) to Y.D. and a Swiss National Science Foundation grant  
530 (310030\_189226) to S.T.P. The authors declare no competing financial interests.

531

532

533

534

535

### 536 **References**

537

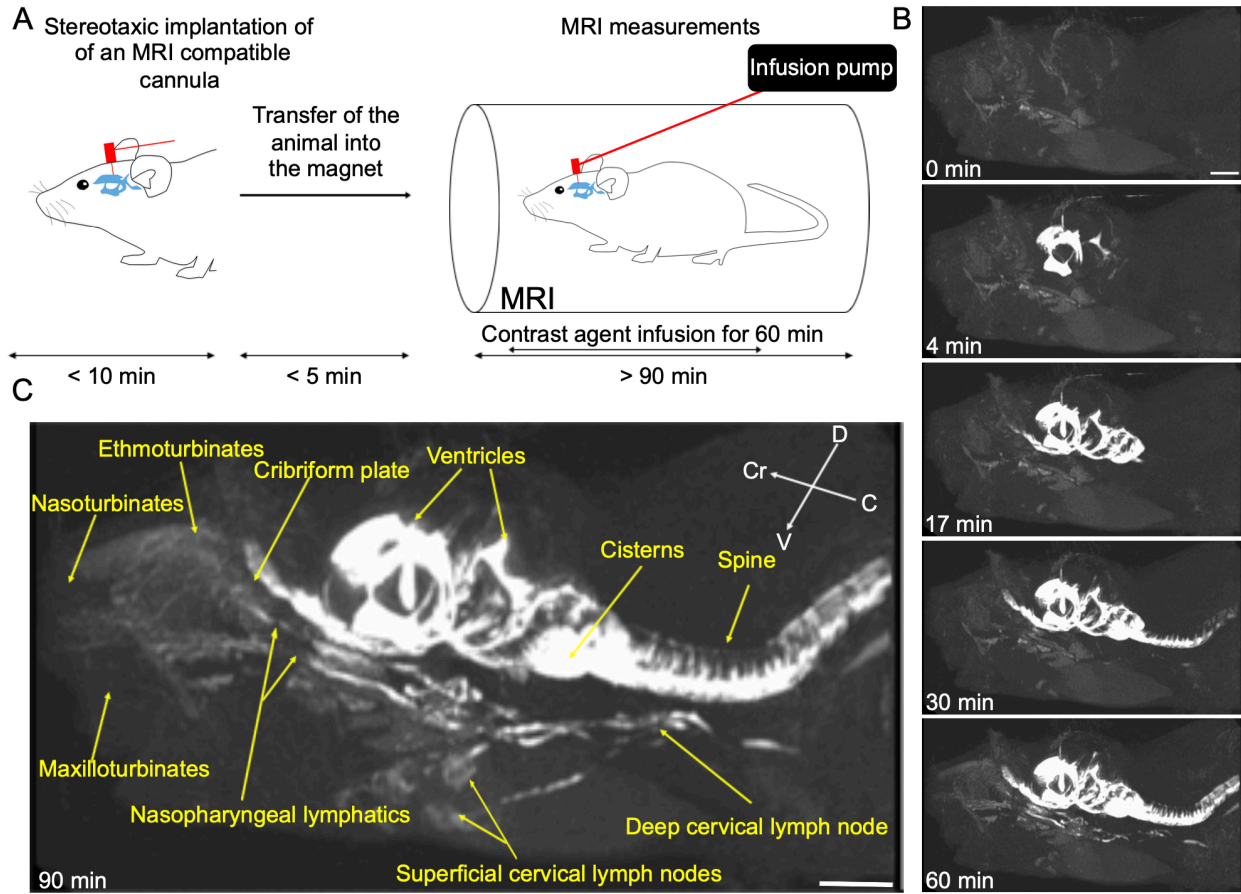
- 538 1. Weed LH. Studies on cerebro-spinal fluid. No. IV : The dual source of cerebro-  
539 spinal fluid. *J Med Res.* 1914;31(1):93-118 11.
- 540 2. Davson H, and Segal MB. *Physiology of the CSF and blood-brain barriers.* Boca  
541 Raton etc.: CRC Press; 1996.
- 542 3. Bradbury MWB, and Cserr HF. In: Johnston MG ed. *Experimental biology of the*  
543 *lymphatic circulation.* Amsterdam: Elsevier; 1985:355-94.
- 544 4. McComb JG. Recent research into the nature of cerebrospinal fluid formation  
545 and absorption. *J Neurosurg.* 1983;59(3):369-83.
- 546 5. Koh L, et al. Integration of the subarachnoid space and lymphatics: is it time to  
547 embrace a new concept of cerebrospinal fluid absorption? *Cerebrospinal Fluid*  
548 *Res.* 2005;2:6.
- 549 6. Proulx ST. Cerebrospinal fluid outflow: a review of the historical and  
550 contemporary evidence for arachnoid villi, perineural routes, and dural  
551 lymphatics. *Cell Mol Life Sci.* 2021.
- 552 7. Ma Q, et al. Outflow of cerebrospinal fluid is predominantly through lymphatic  
553 vessels and is reduced in aged mice. *Nat Commun.* 2017;8(1):1434.
- 554 8. Ma Q, et al. Rapid lymphatic efflux limits cerebrospinal fluid flow to the brain.  
555 *Acta Neuropathol.* 2019;137(1):151-65.

- 556 9. Louveau A, et al. Structural and functional features of central nervous system  
557 lymphatic vessels. *Nature*. 2015;523(7560):337-41.
- 558 10. Aspelund A, et al. A dural lymphatic vascular system that drains brain interstitial  
559 fluid and macromolecules. *J Exp Med*. 2015;212(7):991-9.
- 560 11. Ahn JH, et al. Meningeal lymphatic vessels at the skull base drain cerebrospinal  
561 fluid. *Nature*. 2019;572:62-6.
- 562 12. Pizzo ME, et al. Intrathecal antibody distribution in the rat brain: surface diffusion,  
563 perivascular transport and osmotic enhancement of delivery. *J Physiol*.  
564 2018;596(3):445-75.
- 565 13. Ma Q, et al. Clearance of cerebrospinal fluid from the sacral spine through  
566 lymphatic vessels. *J Exp Med*. 2019;216(11):2492-502.
- 567 14. Brady M, et al. Cerebrospinal fluid drainage kinetics across the cribriform plate  
568 are reduced with aging. *Fluids Barriers CNS*. 2020;17(1):71.
- 569 15. Stanton EH, et al. Mapping of CSF transport using high spatiotemporal resolution  
570 dynamic contrast-enhanced MRI in mice: Effect of anesthesia. *Magn Reson Med*.  
571 2021.
- 572 16. Faber WM. The nasal mucosa and the subarachnoid space. *Am J Anat*.  
573 1937;62(1):121-48.
- 574 17. Erlich SS, et al. Ultrastructural morphology of the olfactory pathway for  
575 cerebrospinal fluid drainage in the rabbit. *J Neurosurg*. 1986;64(3):466-73.
- 576 18. Kida S, et al. CSF drains directly from the subarachnoid space into nasal  
577 lymphatics in the rat. Anatomy, histology and immunological significance.  
578 *Neuropathol Appl Neurobiol*. 1993;19(6):480-8.
- 579 19. Norwood JN, et al. Anatomical basis and physiological role of cerebrospinal fluid  
580 transport through the murine cribriform plate. *eLife*. 2019;8:1-32.
- 581 20. Hsu M, et al. Neuroinflammation-induced lymphangiogenesis near the cribriform  
582 plate contributes to drainage of CNS-derived antigens and immune cells. *Nat*  
583 *Commun*. 2019;10(1):229.
- 584 21. Mortensen AO, and Sullivan WE. The cerebrospinal fluid and the cervical lymph  
585 nodes. *Anat Rec*. 1933;56(4):359-63.
- 586 22. Pile-Spellman JM, et al. Experimental in vivo imaging of the cranial perineural  
587 lymphatic pathway. *AJNR Am J Neuroradiol*. 1984;5(5):539-45.
- 588 23. Kwon S, et al. Fluorescence imaging of lymphatic outflow of cerebrospinal fluid in  
589 mice. *J Immunol Methods*. 2017;449:37-43.
- 590 24. Yamada S, et al. MRI tracer study of the cerebrospinal fluid drainage pathway in  
591 normal and hydrocephalic guinea pig brain. *Tokai J Exp Clin Med*. 2005;30(1):21-  
592 9.
- 593 25. Hladky SB, and Barrand MA. Mechanisms of fluid movement into, through and  
594 out of the brain: evaluation of the evidence. *Fluids Barriers CNS*. 2014;11(1):26.
- 595 26. Steffensen AB, et al. Cotransporter-mediated water transport underlying  
596 cerebrospinal fluid formation. *Nat Commun*. 2018;9(1):2167.
- 597 27. Liu G, et al. Direct Measurement of Cerebrospinal Fluid Production in Mice. *Cell*  
598 *Rep*. 2020;33(12):108524.

- 599 28. Louveau A, et al. CNS lymphatic drainage and neuroinflammation are regulated  
600 by meningeal lymphatic vasculature. *Nat Neurosci.* 2018;21(10):1380-91.
- 601 29. Rustenhoven J, et al. Functional characterization of the dural sinuses as a  
602 neuroimmune interface. *Cell.* 2021.
- 603 30. Oliver G, et al. The Lymphatic Vasculature in the 21(st) Century: Novel  
604 Functional Roles in Homeostasis and Disease. *Cell.* 2020;182(2):270-96.
- 605 31. Iliff JJ, et al. Brain-wide pathway for waste clearance captured by contrast-  
606 enhanced MRI. *J Clin Invest.* 2013;123(3):1299-309.
- 607 32. Lee H, et al. The Effect of Body Posture on Brain Glymphatic Transport. *J*  
608 *Neurosci.* 2015;35(31):11034-44.
- 609 33. Gakuba C, et al. General anesthesia inhibits the activity of the "glymphatic  
610 system". *Theranostics.* 2018;8(3):710-22.
- 611 34. Gaberel T, et al. Impaired glymphatic perfusion after strokes revealed by  
612 contrast-enhanced MRI: a new target for fibrinolysis? *Stroke.* 2014;45(10):3092-  
613 6.
- 614 35. Ringstad G, et al. Brain-wide glymphatic enhancement and clearance in humans  
615 assessed with MRI. *JCI Insight.* 2018;3(13).
- 616 36. Xue Y, et al. In vivo T1 mapping for quantifying glymphatic system transport and  
617 cervical lymph node drainage. *Sci Rep.* 2020;10(1):14592.
- 618 37. Ringstad G, and Eide PK. Cerebrospinal fluid tracer efflux to parasagittal dura in  
619 humans. *Nat Commun.* 2020;11(1):354.
- 620 38. Gherzi-Egea JF, et al. Rapid distribution of intraventricularly administered  
621 sucrose into cerebrospinal fluid cisterns via subarachnoid velae in rat.  
622 *Neuroscience.* 1996;75(4):1271-88.
- 623 39. Mestre H, et al. Flow of cerebrospinal fluid is driven by arterial pulsations and is  
624 reduced in hypertension. *Nat Commun.* 2018;9(1):4878.
- 625 40. Bedussi B, et al. Paravascular spaces at the brain surface: Low resistance  
626 pathways for cerebrospinal fluid flow. *J Cereb Blood Flow Metab.*  
627 2018;38(4):719-26.
- 628 41. Nagra G, and Johnston MG. Impact of ageing on lymphatic cerebrospinal fluid  
629 absorption in the rat. *Neuropathol Appl Neurobiol.* 2007;33(6):684-91.
- 630 42. Preston JE. Ageing choroid plexus-cerebrospinal fluid system. *Microsc Res*  
631 *Tech.* 2001;52(1):31-7.
- 632 43. Karaman S, et al. Decline of lymphatic vessel density and function in murine skin  
633 during aging. *Angiogenesis.* 2015;18(4):489-98.
- 634 44. Proulx ST, et al. Quantitative measurement of lymphatic function in mice by  
635 noninvasive near-infrared imaging of a peripheral vein. *JCI Insight.*  
636 2017;2(1):e90861.
- 637 45. Zolla V, et al. Aging-related anatomical and biochemical changes in lymphatic  
638 collectors impair lymph transport, fluid homeostasis, and pathogen clearance.  
639 *Aging Cell.* 2015;14(4):582-94.
- 640 46. Da Mesquita S, et al. Functional aspects of meningeal lymphatics in ageing and  
641 Alzheimer's disease. *Nature.* 2018;560(7717):185-91.



642 47. Schwalbe G. Die Arachnoidalraum ein Lymphraum und sein Zusammenhang mit  
643 den Perichoroidalraum. [The arachnoidal space as a lymphatic space with  
644 connection to the perichoroidal compartment.]. *Zbl med Wiss* 1869;7:465–7.  
645 48. Erlich SS, et al. Ultrastructure of the orbital pathway for cerebrospinal fluid  
646 drainage in rabbits. *J Neurosurg.* 1989;70(6):926-31.  
647 49. Ludemann W, et al. Ultrastructure of the cerebrospinal fluid outflow along the  
648 optic nerve into the lymphatic system. *Child Nerv Syst.* 2005;21(2):96-103.  
649 50. Brierley JB, and Field EJ. The connexions of the spinal sub-arachnoid space with  
650 the lymphatic system. *J Anat.* 1948;82(3):153-66.  
651 51. Marmarou A, et al. Compartmental analysis of compliance and outflow resistance  
652 of the cerebrospinal fluid system. *J Neurosurg.* 1975;43:523-34.  
653 52. Bozanovic-Sosic R, et al. Spinal and cranial contributions to total cerebrospinal  
654 fluid transport. *Am J Physiol-Reg I.* 2001;281(3):R909-R16.  
655 53. Bradbury MW, and Westrop RJ. Factors influencing exit of substances from  
656 cerebrospinal fluid into deep cervical lymph of the rabbit. *J Physiol.*  
657 1983;339:519-34.  
658 54. Johnston M, et al. Evidence of connections between cerebrospinal fluid and  
659 nasal lymphatic vessels in humans, non-human primates and other mammalian  
660 species. *Cerebrospinal Fluid Res.* 2004;1(1):2.  
661 55. Mollanji R, et al. Intracranial pressure accommodation is impaired by blocking  
662 pathways leading to extracranial lymphatics. *Am J Physiol Regul Integr Comp*  
663 *Physiol.* 2001;280(5):R1573-81.  
664 56. Hablitz LM, et al. Increased glymphatic influx is correlated with high EEG delta  
665 power and low heart rate in mice under anesthesia. *Sci Adv.*  
666 2019;5(2):eaav5447.  
667 57. Voelz K, et al. A ferritin tracer study of compensatory spinal CSF outflow  
668 pathways in kaolin-induced hydrocephalus. *Acta Neuropathol.* 2007;113(5):569-  
669 75.  
670 58. Ma Q, et al. Lymphatic outflow of cerebrospinal fluid is reduced in glioma. *Sci*  
671 *Rep.* 2019;9(1):14815.  
672 59. Lowhagen P, et al. The Nasal Route of Cerebrospinal-Fluid Drainage in Man - a  
673 Light-Microscope Study. *Neuropathol Appl Neurobiol.* 1994;20(6):543-50.  
674 60. de Leon MJ, et al. Cerebrospinal Fluid Clearance in Alzheimer Disease  
675 Measured with Dynamic PET. *J Nucl Med.* 2017;58(9):1471-6.  
676 61. Melin E, et al. In vivo assessment of cerebrospinal fluid efflux to nasal mucosa in  
677 humans. *Sci Rep.* 2020;10(1):14974.  
678 62. Muller A, et al. Magnetic resonance lymphography at 9.4 T using a Gadolinium-  
679 based nanoparticle in rats. Investigations in healthy animals and in a hindlimb  
680 lymphedema model. *Invest Radiol.* 2017;52(12):725-33.  
681  
682  
683  
684  
685  
686



687  
 688  
 689  
 690  
 691  
 692  
 693  
 694  
 695  
 696  
 697  
 698  
 699  
 700  
 701  
 702  
 703  
 704  
 705  
 706  
 707  
 708  
 709  
 710  
 711  
 712

**Figure 1: Dynamic CE-MRI shows continuous efflux of contrast agent from the nasal region through lymphatic vessels to cervical lymph nodes following low-rate ventricular infusion.** **A** Schematic representation of the experimental setup. MRI-compatible cannulae were stereotactically implanted into the ventricle of 2-3 months old C57BL/6J mice anesthetized with ketamine/xylazine. The animals were then transferred into a horizontal-bore 9.4 T MRI. Polyethylene tubing containing the contrast agent (Gadospin D solution at 25 mM Gd) was attached connecting the cannula and the infusion pump. Before tracer infusion, T1-weighted (3D time-of-flight gradient recalled echo sequence) MRI measurements were started and followed by intraventricular low-rate infusion (0.1  $\mu\text{l}/\text{min}$ ) of the tracer while MRI acquisitions continued. **B** Representative signal dynamics using maximum-intensity projections visualizing the entire head-neck region. Following the beginning of contrast agent infusion, enhancement of the signal intensity in the ventricle is detectable at 4 min, in the nasal cavity at 17 min, and in the neck lymph nodes at 30 and 60 min. **C** Visualization of the spread of tracer after 90 min demonstrating continuous signal enhancement from the cribriform plate to the nasopharyngeal lymphatic vessels to cervical lymph nodes. Data are representative of  $n = 7$  mice and three independent experiments. Scale bars: 3 mm.

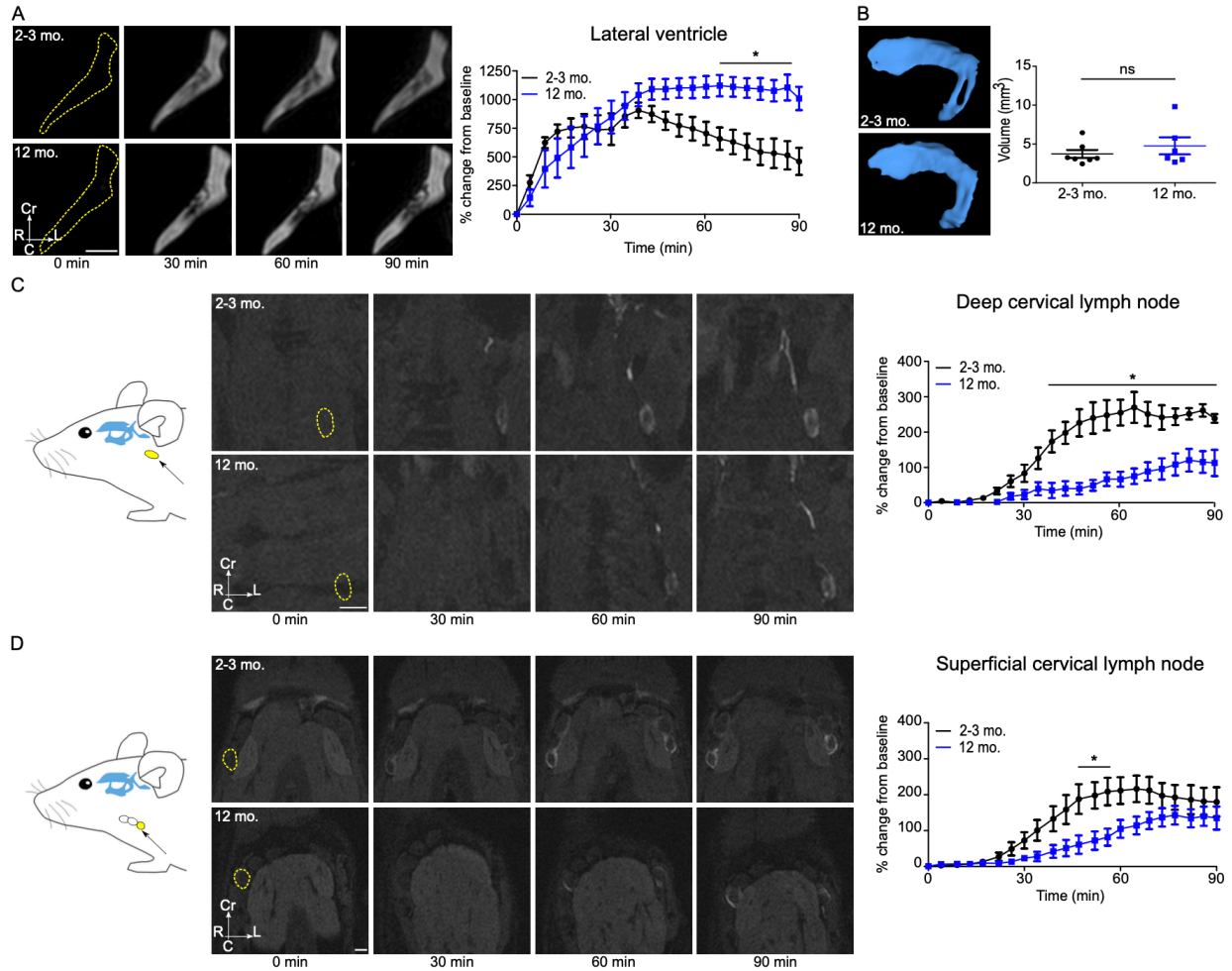
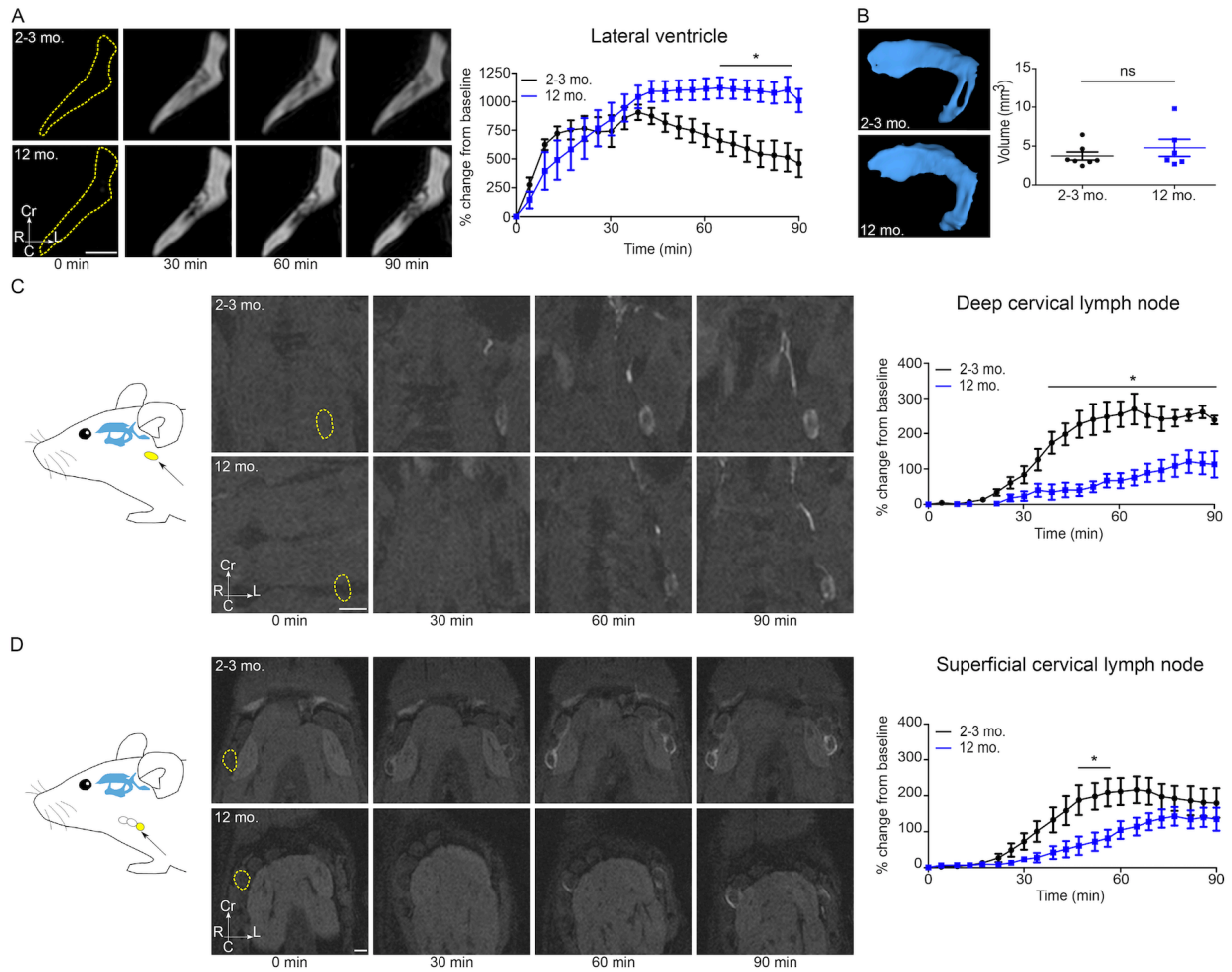


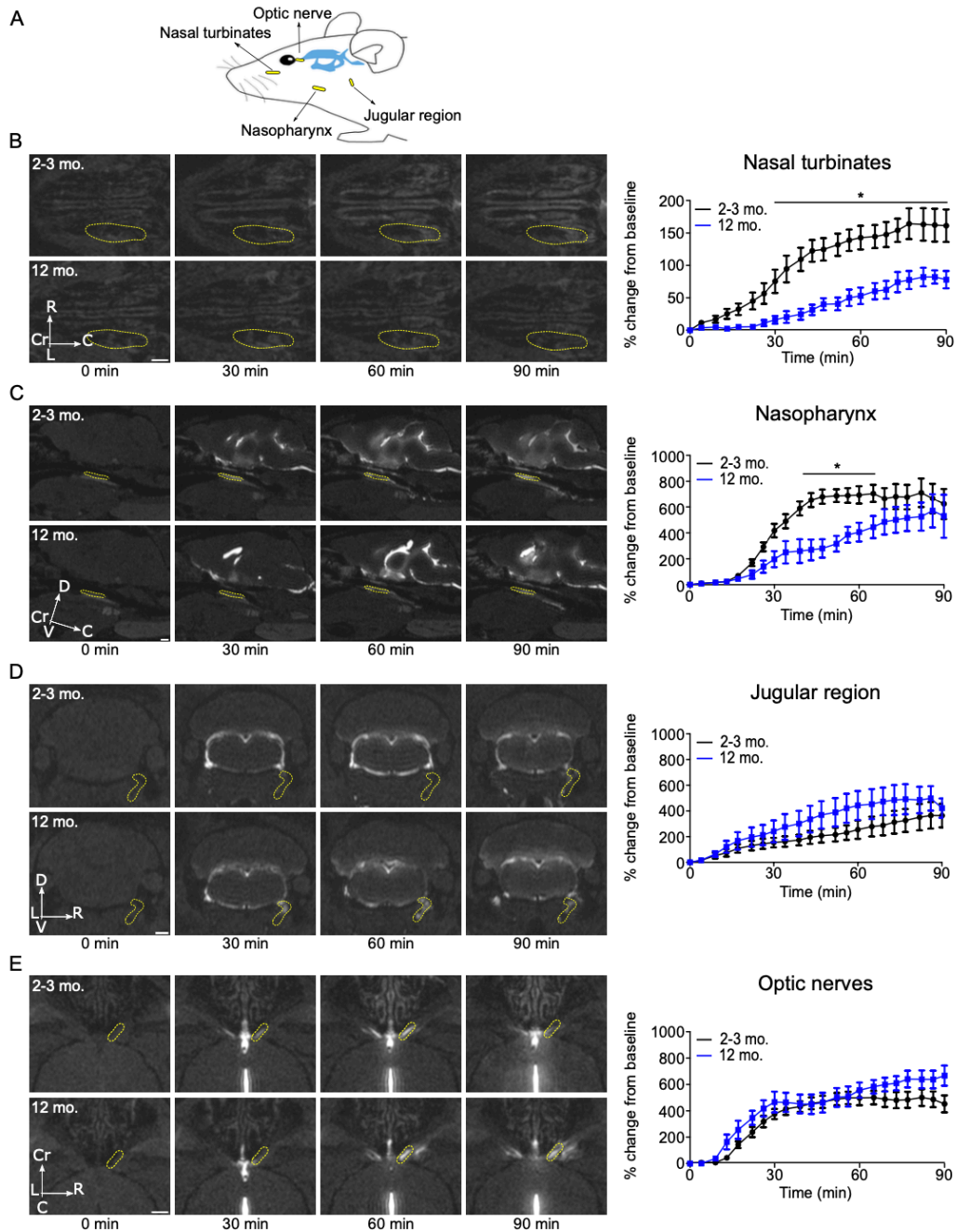
**Figure 2: Clearance from ventricles and efflux to lymph nodes are reduced in 12 months old mice.** Visualization of tracer spread after low-rate intraventricular infusion (0.1  $\mu\text{l}/\text{min}$ ) of a Gadospin D solution at 25 mM; data acquired with a series of T1-weighted MRI measurements (3D time-of-flight gradient recalled echo sequence). **A** Signal dynamics of Gadospin D contrast agent showing clearance from the contralateral-ventricles in the horizontal plane in 2-3 months and 12 months old mice. **B** Representative images of 3D reconstruction of the contralateral-ventricles of 2-3 months and 12 months old mice. Ventricle volumes of 2-3 months and 12 months old mice were compared with two-tailed Student's t-test. **C-D** Signal dynamics in the horizontal plane of Gadospin D tracer efflux to deep and superficial cervical lymph nodes in 2-3 months and 12 months old mice. ROIs shown in yellow. Data are expressed as mean  $\pm$  SEM of  $n=7$  2-3 months old mice vs  $n=6$  12 months old mice and are representative of three independent experiments.. \* $p<0.05$  (two-way ANOVA followed by Bonferroni's posthoc test). Scale bars: 1 mm.

713  
714  
715  
716  
717  
718  
719  
720  
721  
722  
723  
724  
725  
726  
727  
728  
729  
730  
731  
732  
733  
734  
735



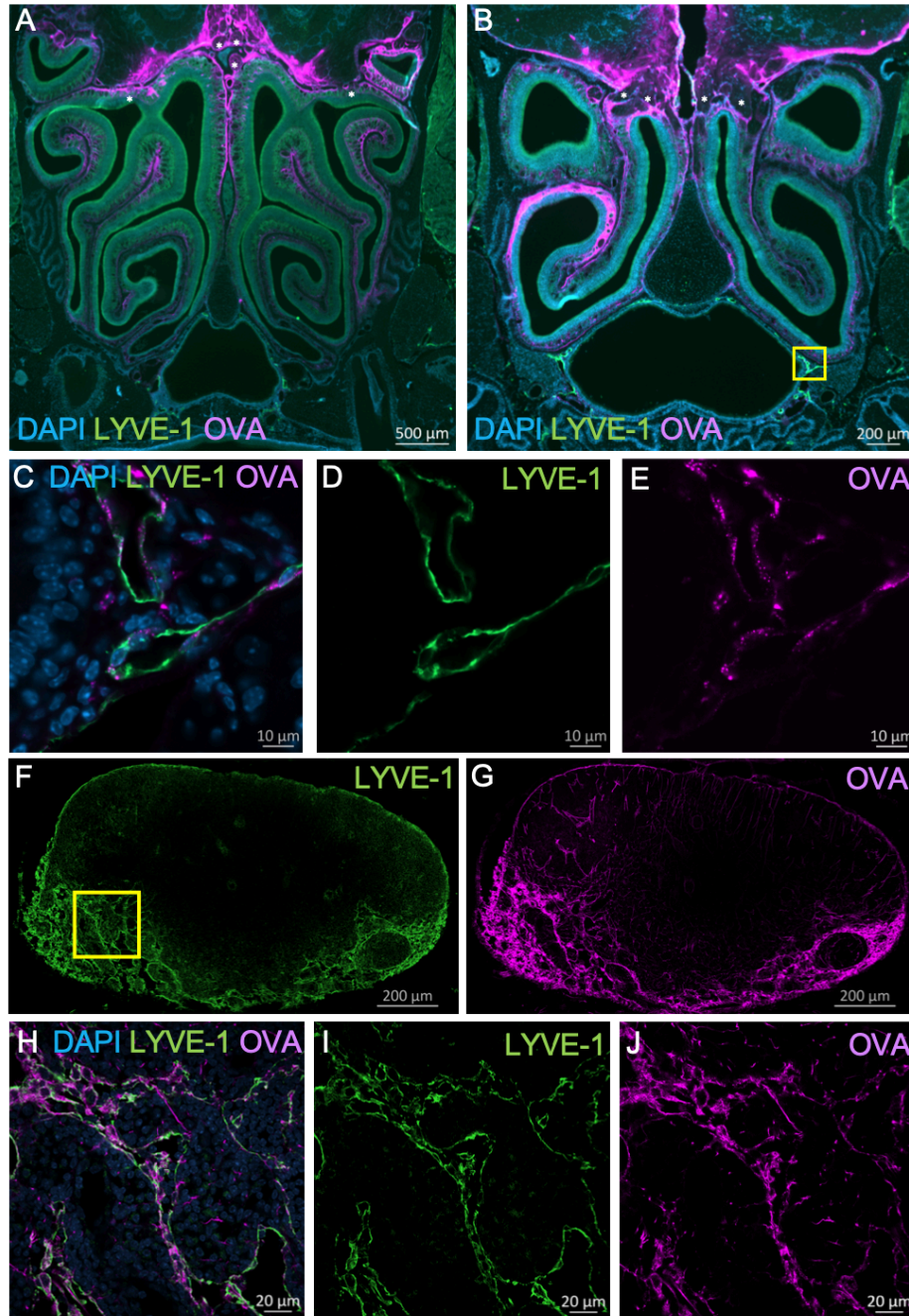
736  
737  
738  
739  
740  
741  
742  
743  
744  
745  
746  
747  
748  
749  
750  
751  
752  
753  
754  
755  
756  
757  
758

**Figure 3: CSF predominantly clears along the ventral aspect of the skull.** Visualization of tracer clearance after low-rate intraventricular infusion (0.1  $\mu$ l/min) of Gadospin D solution at 25 mM Gd. Data were acquired with a series of T1-weighted MRI measurements (3D time-of-flight gradient recalled echo sequence). **A** Overview scheme of ROI location. **B,C** Coronal sections demonstrating in 2-3 months and 12 months old mice the dynamics of CSF efflux in representative ROIs (shown in yellow) of the dorsal aspect of the skull: in the perisagittal superior sinus and the quadrigeminal cisterns. **D,E** Horizontal sections showing the dynamic of CSF efflux in the ventral aspect of the skull in 2-3 months and 12 months old mice: around the circle of Willis and around the internal carotid (ROIs in yellow). Quantifications of the different ROIs are expressed as the mean  $\pm$  SEM of n=7 2-3 months old mice vs n=6 12 months old mice and are representative of three independent experiments. \*p<0.05, (two-way ANOVA followed by Bonferroni's posthoc test). Scale bars: 1 mm.



759  
760 **Figure 4: Clearance of CSF from the cranium is reduced with aging in the nasal turbinates and the**  
761 **nasopharynx but not in the jugular region and around the optic nerves.** Imaging of tracer clearance  
762 after low-rate intraventricular infusion (0.1  $\mu\text{l}/\text{min}$ ) of Gadospin D solution at 25 mM Gd. Data were acquired  
763 with a series of T1-weighted MRI measurements (3D time-of-flight gradient recalled echo sequence). **A**  
764 Overview scheme of ROI location. **B** Horizontal sections demonstrating the dynamics of CSF efflux to nasal  
765 turbinates in 2-3 months and 12 months old mice. **C** Sagittal sections reveal the dynamics of contrast agent  
766 in the nasopharynx in the two groups of mice. **D** Coronal sections demonstrating the CSF efflux from the  
767 jugular region in the groups of mice of different ages. **E** Horizontal sections showing CSF efflux along the  
768 optic nerve in 2-3 months and 12 months old mice. Quantifications of the different ROIs (shown in yellow)  
769 are expressed as the mean  $\pm$  SEM of  $n=7$  2-3 months old mice vs  $n=6$  12 months old mice and are  
770 representative of three independent experiments. \* $p<0.05$  (two-way ANOVA followed by Bonferroni's  
771 posthoc test). Scale bars: 1 mm.





772  
773  
774  
775  
776  
777  
778  
779  
780  
781  
782  
783  
784

**Figure 5: Histological validation of CSF tracer efflux through the cribriform plate to nasopharyngeal lymphatics and to deep cervical lymph nodes.** Fluorescently-labeled ovalbumin (OVA) was introduced via low-rate intraventricular infusion (0.1 μl/min for 60 min) and at 90 min the mice were sacrificed for post-mortem analysis of tracer efflux. **A, B** Coronal sections of decalcified skulls demonstrating significant efflux of OVA into the nasal mucosal tissues. OVA (purple) can be seen crossing the cribriform plate alongside several olfactory nerve bundles (indicated with \*). Lymphatic vessels (stained with LYVE-1 in green) can be found in proximity to the nasopharynx under the nasal turbinates. **C-E** High-magnification view of the nasopharyngeal region indicated by the yellow box in B, demonstrating OVA signal within the LYVE-1<sup>+</sup> lymphatic vessels. **F, G** Sections of deep cervical lymph nodes indicating close association of OVA signal within lymphatic sinuses stained with LYVE-1. **H-J** High-magnification view of the region indicated by the yellow box in F, demonstrating OVA signal within the LYVE-1<sup>+</sup> lymphatic sinuses. Data are representative of n = 6 mice and two independent experiments.